

Competition between Charge Density Wave and Superconductivity in a Janus MXene Mo_2NF_2

Jakkapat Seeyangnok^{1a}, Udomsilp Pinsook^{1b}, Graeme J Ackland^{2c}

¹Department of Physics, Faculty of Science,
Chulalongkorn University, Bangkok, Thailand

²Centre for Science at Extreme Conditions,
School of Physics and Astronomy,
University of Edinburgh, Edinburgh, United Kingdom

^ajakkapatjpt@gmail.com

^budomsilp.p@chula.ac.th

^cgjackland@ed.ac.uk

Abstract

Charge-density-wave (CDW) order and superconductivity often compete in low-dimensional materials, yet their interplay in Janus MXenes remains largely unexplored. Here, we present a comprehensive first-principles investigation of the structural, vibrational, and electronic properties of Mo_2NF_2 . Phonon calculations reveal an unstable soft phonon mode at the M point in the high-symmetry structure, signaling a CDW instability. Analysis of phonon linewidths and the real and imaginary parts of the bare electronic susceptibility demonstrates that the CDW is not driven by simple Fermi-surface nesting but instead originates from strong momentum-dependent electron-phonon coupling. Structural relaxation yields a commensurate CDW phase characterized by bond-length modulations involving the Mo, N, and F sublattices. We further show that charge doping alone is insufficient to stabilize the soft phonon, whereas compressive biaxial strain exceeding -3% completely suppresses the CDW instability. Electron-phonon coupling calculations indicate that the CDW phase exhibits a reduced coupling constant $\lambda = 0.40$ and logarithmic phonon frequency $\omega_{\log} = 219$ K, leading to a low superconducting transition temperature of $T_c \sim 1$ K. In contrast, the strain-stabilized high-symmetry phase shows enhanced coupling ($\lambda = 0.53$, $\omega_{\log} = 272$ K) and a higher $T_c \sim 4$ K. Our results establish Mo_2NF_2 as a strain-tunable platform where superconductivity emerges upon suppression of a competing CDW phase, highlighting the crucial role of lattice control in Janus MXenes.

Keywords: Charge-density wave; Janus MXenes; Electron-phonon coupling; Strain engineering; Superconductivity; Phonon instability; Two-dimensional materials

1 Introduction

Charge-density-wave (CDW) order represents a fundamental manifestation of collective behavior in low-dimensional solids, arising from the coupled reorganization of electronic states and the crystal lattice. A CDW state is characterized by a periodic modulation of the electronic charge density that is accompanied by a symmetry-breaking lattice distortion, reflecting the intimate interplay between electrons and phonons in reduced dimensions [1]. The earliest theoretical description of CDWs was provided by

Peierls in the context of one-dimensional metallic systems, where perfect nesting of the Fermi surface produces a divergence in the electronic susceptibility and drives a lattice instability at a characteristic wave vector [2]. This electronic instability is inherently linked to phonon softening via electron–phonon coupling, a mechanism later formalized through the concept of the Kohn anomaly [3].

While the Peierls framework provides an elegant description of CDW formation in idealized one-dimensional systems, it has become increasingly clear that this picture is insufficient to explain CDW phenomena in higher dimensions. In quasi-two-dimensional materials, the Fermi surface typically lacks the perfect nesting required to sustain a purely electronic instability. Instead, both experimental observations and first-principles calculations have demonstrated that CDW transitions in realistic materials are governed by a cooperative interaction between electronic states and lattice degrees of freedom, mediated by a strongly momentum-dependent electron–phonon coupling [4,5]. In this scenario, selective softening of specific phonon modes at well-defined wave vectors plays a decisive role, and the CDW transition is best understood as a coupled electronic–structural instability rather than a purely electronic Peierls transition [5].

Layered transition-metal dichalcogenides (TMDs) provide a paradigmatic class of materials for investigating CDW physics in two dimensions. Prototypical compounds such as NbSe₂ [6–9], TaSe₂ [4,9,10], and TaS₂ [11–13] exhibit robust CDW phases despite the absence of pronounced Fermi-surface nesting. In these systems, detailed momentum-resolved studies have established that the CDW instability originates from highly anisotropic electron–phonon coupling, which selectively enhances phonon softening at specific wave vectors and stabilizes symmetry-lowering lattice distortions [7,14]. The weak inter-layer coupling in TMDs further enables the persistence of CDW order down to the monolayer limit, where genuinely two-dimensional CDW phases have been experimentally realized [8,10]. In hydrogen-functionalized TMDs, MoSH has been proposed to exhibit stronger lattice instabilities in the 1T phase, which may be associated with charge-density-wave (CDW) formation [15] and in its bilayer configuration [16]. More recently, signatures of CDW ordering have been observed in both the 2H and 1T phases of MoSeH [17]. Charge-density-wave (CDW) phases in both MoSH and MoSeH have recently been examined in detail [18]. A similar interplay between superconductivity and CDW distortions has been suggested for hydrogen-functionalized Janus systems such as WSH and WSeH, where superconductivity with T_c values on the order of 10–15 K coexists with structural modulations characteristic of CDW ordering [19–21]. Furthermore, several Janus group-IV transition-metal MXH monolayers have been theoretically investigated and predicted to host phonon-mediated superconductivity with T_c ranging from 9 to 30 K [22–24]. Importantly, some of these hydrogen-functionalized systems also display lattice instabilities indicative of competing CDW phases, similar to those identified in MoSH-, WSH-, and WSeH-based monolayers, highlighting the delicate balance between superconductivity and structural ordering in this class of materials. As a result, TMDs have emerged as an ideal platform for exploring CDW formation beyond one dimension and for examining its competition and coexistence with other collective phenomena, most notably superconductivity.

In contrast to other halogen-functionalized systems, halogen functionalization in Mo₂C has been shown to enhance superconductivity [25]. In this work, we present a comprehensive first-principles study of the charge-density-wave (CDW) instability and its interplay with superconductivity in Mo₂NF₂. By combining phonon dispersion, phonon linewidth analysis, and momentum-resolved electronic susceptibility, we identify a soft phonon mode at the *M* point as the microscopic origin of the CDW instability, driven by strong momentum-dependent electron-phonon coupling rather than Fermi-surface nesting. We further resolve the real-space CDW structure and reveal cooperative lattice distortions of the Mo, N, and F sublattices. Moreover, we show that external perturbations affect the instability differently: charge doping fails to stabilize the soft mode, whereas moderate compressive biaxial strain suppresses the CDW, restores the high-symmetry phase, and enhances electron-phonon coupling, significantly increasing the

superconducting transition temperature. These results establish strain as an effective parameter for tuning competing collective phases in Janus MXenes and deepen the understanding of lattice-driven CDW physics in two-dimensional materials.

2 Computational Methods

First-principles calculations were performed within density functional theory (DFT) as implemented in the QUANTUM ESPRESSO package [26]. The exchange–correlation functional was treated using the generalized gradient approximation in the Perdew–Burke–Ernzerhof (GGA-PBE) form [27]. Optimized norm-conserving Vanderbilt pseudopotentials [28] were employed for all atomic species. The kinetic-energy cutoffs for the plane-wave basis set and charge density were set to 80 Ry and 320 Ry, respectively.

Structural optimizations were carried out by fully relaxing atomic positions and lattice parameters until the residual forces on each atom were below 10^{-5} eV/Å. Brillouin-zone integrations for self-consistent calculations were performed using Monkhorst–Pack \mathbf{k} -point meshes [29] of $24 \times 24 \times 1$ for the primitive unit cell, together with Methfessel–Paxton smearing [30] of width 0.02 Ry. For supercell calculations, the \mathbf{k} -point meshes were reduced proportionally to the supercell size, corresponding to $12 \times 12 \times 1$, $9 \times 9 \times 1$, $6 \times 6 \times 1$, and $3 \times 3 \times 1$ meshes for $2 \times 2 \times 1$, $3 \times 3 \times 1$, $4 \times 4 \times 1$, and $5 \times 5 \times 1$ supercells, respectively.

Several magnetic configurations were examined to determine the magnetic ground state of Mo₂NF₂ MXenes. These include a ferromagnetic (FM) configuration, in which the initial magnetic moments of all Mo atoms were aligned parallel, as well as antiferromagnetic (AFM) configurations. The AFM states considered consist of a G-type antiferromagnetic (GAF) ordering, characterized by antiparallel alignment between neighboring Mo atoms, and an A-type antiferromagnetic (AAF) ordering, where spins are aligned ferromagnetically within the lower Mo plane but antiparallel to those in the upper Mo plane. The calculations indicate that none of the magnetic configurations stabilize a magnetic insulating phase. Instead, Mo₂NF₂ MXenes favor a metallic ground state regardless of the initial magnetic ordering. This behavior suggests that itinerant electronic states dominate near the Fermi level, suppressing long-range magnetic ordering in the high-symmetry phase.

Phonon dispersions and lattice dynamical properties were calculated within density functional perturbation theory (DFPT) [31]. Dynamical matrices were computed on uniform $12 \times 12 \times 1$ \mathbf{q} -point meshes for the primitive unit cell and on $6 \times 6 \times 1$ meshes for the $2 \times 2 \times 1$ CDW supercells. Dynamical stability was assessed by inspecting the phonon spectra for imaginary frequencies. Electron–phonon interactions were evaluated within the density functional perturbation theory (DFPT) framework [31].

The superconducting transition temperature T_c was evaluated within the Allen–Dynes formalism using the isotropic Eliashberg spectral function $\alpha^2F(\omega)$ [32, 33]. It is given by

$$T_c = \frac{\omega_{\text{ln}}}{1.2} \exp \left[-\frac{1.04(1 + \lambda)}{\lambda - \mu^*(1 + 0.62\lambda)} \right], \quad (1)$$

where λ denotes the electron–phonon coupling (EPC) constant and μ^* is the Coulomb pseudopotential.

The EPC constant λ is obtained from the Eliashberg spectral function as

$$\lambda = 2 \int_0^\infty \frac{\alpha^2F(\omega)}{\omega} d\omega. \quad (2)$$

The logarithmic average phonon frequency ω_{ln} , which characterizes the effective phonon energy scale, is defined as

$$\omega_{\text{ln}} = \exp \left[\frac{2}{\lambda} \int_0^\infty \frac{\alpha^2F(\omega)}{\omega} \ln \omega d\omega \right]. \quad (3)$$

In addition, the second moment of the phonon spectrum ω_2 is expressed as

$$\omega_2 = \left[\frac{2}{\lambda} \int_0^\infty \alpha^2 F(\omega) \omega d\omega \right]^{1/2}. \quad (4)$$

3 Results and Discussion

3.1 High-symmetry structure (HSS)

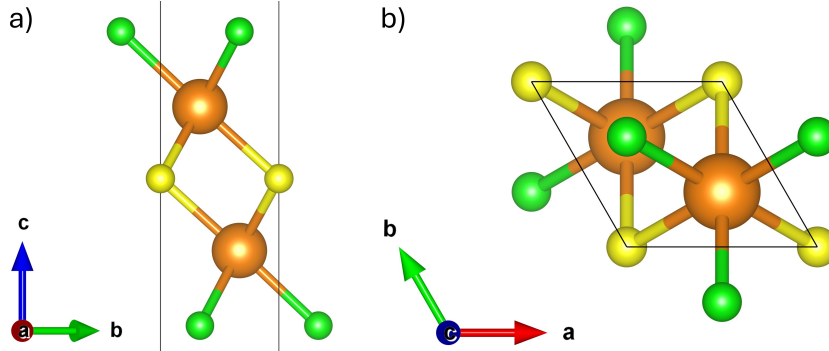


Figure 1: (a) Side and (b) top views of the optimized crystal structure of the Mo_2NF monolayer. Orange, yellow, and green spheres represent Mo, N, and F atoms, respectively.

The high-symmetry phase of Mo_2NF_2 MXene was investigated within a hexagonal lattice framework. The optimized structure crystallizes in the centrosymmetric space group $P\bar{3}m1$ (No. 164) with an extended Bravais lattice symbol of hP2. To model the two-dimensional geometry, a vacuum spacing of 20.0 Å was introduced along the out-of-plane (c) direction to eliminate spurious interactions between periodic images. In this structure, the nitrogen atom occupies the $1b$ Wyckoff position at $(0, 0, 0.5)$, forming the central atomic layer. The Mo atoms are located at the $2d$ Wyckoff positions with fractional coordinates $(2/3, 1/3, z)$ and $(1/3, 2/3, 1 - z)$, where $z = 0.5726$, resulting in two Mo layers symmetrically displaced about the N plane. The F surface terminations also occupy the $2d$ Wyckoff sites at $(1/3, 2/3, z_F)$ and $(2/3, 1/3, 1 - z_F)$ with $z_F = 0.6484$, leading to symmetric functionalization on both sides of the MXene sheet. The optimized in-plane lattice constant is $a = 2.76$ Å. Upon fluorine functionalization, the system becomes thermodynamically more stable, with a binding energy of -9.41 eV/formula, and exhibits a metallic ground-state configuration.

To elucidate the microscopic origin of the charge-density-wave (CDW) instability in Fluorine-Functionalized Mo_2N , we analyze the phonon dispersions, phonon linewidths, and the real and imaginary parts of the bare electronic susceptibility, as summarized in Fig. 2. This combined analysis enables us to distinguish between a CDW driven by Fermi-surface nesting and one originating from momentum-dependent electron-phonon coupling. The bare (Lindhard) electronic susceptibility is given by

$$\text{Re}[\chi(\mathbf{q}, \omega)] = \sum_{\mathbf{k}} \frac{f(\varepsilon_{\mathbf{k}}) - f(\varepsilon_{\mathbf{k}+\mathbf{q}})}{\omega + \varepsilon_{\mathbf{k}} - \varepsilon_{\mathbf{k}+\mathbf{q}}}, \quad (5)$$

$$\text{Im}[\chi(\mathbf{q}, \omega)] = \pi \sum_{\mathbf{k}} [f(\varepsilon_{\mathbf{k}}) - f(\varepsilon_{\mathbf{k}+\mathbf{q}})] \delta(\omega + \varepsilon_{\mathbf{k}} - \varepsilon_{\mathbf{k}+\mathbf{q}}), \quad (6)$$

where $\varepsilon_{\mathbf{k}}$ denotes the electronic band energy and $f(\varepsilon)$ is the Fermi-Dirac distribution function.

In the static limit ($\omega \rightarrow 0$), the imaginary part, $\text{Im}[\chi_0(\mathbf{q})] = \text{Im}[\chi(\mathbf{q}, 0)]$, primarily reflects the topology of the Fermi surface and is often used as an indicator of Fermi-surface nesting. In contrast, the

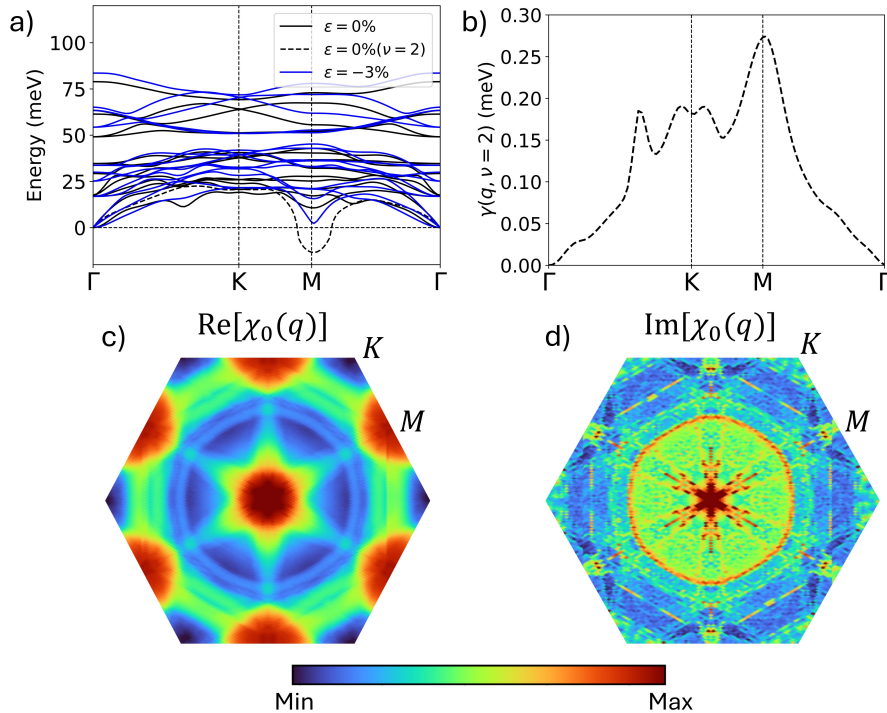


Figure 2: (a) Phonon dispersion along the high-symmetry path Γ - K - M - Γ . The black solid lines correspond to the unstrained structure ($\varepsilon = 0\%$), while the black dashed line ($\nu = 2$) indicates an unstable soft phonon mode at the M point. The blue curves show the phonon dispersion under compressive strain ($\varepsilon = -3\%$), where the soft mode is fully stabilized. (b) Phonon linewidth $\gamma(\mathbf{q}, \nu = 2)$, exhibiting a pronounced enhancement near the M point, indicative of strong electron-phonon coupling. (c) Real part of the static electronic susceptibility, $\text{Re}[\chi_0(\mathbf{q})]$, showing enhanced responses at high-symmetry wave vectors. (d) Imaginary part of the electronic susceptibility, $\text{Im}[\chi_0(\mathbf{q})]$, revealing pronounced features associated with Fermi-surface nesting.

real part, $\text{Re}[\chi_0(\mathbf{q})] = \text{Re}[\chi(\mathbf{q}, 0)]$, governs the stability of the electronic system and directly contributes to the renormalization of phonon frequencies. A pronounced enhancement in $\text{Re}[\chi_0(\mathbf{q})]$ at a particular wave vector can induce phonon softening and drive a structural instability. Consequently, a CDW of purely electronic (Peierls-type) origin requires coincident peaks in both $\text{Re}[\chi_0(\mathbf{q})]$ and $\text{Im}[\chi_0(\mathbf{q})]$ at the same ordering vector \mathbf{q}_{CDW} .

As shown in Fig. 2(a), the phonon spectrum of unstrained Mo_2NF_2 exhibits a pronounced softening of a low-energy phonon branch at the M point, signaling a lattice instability toward a commensurate modulation with $\mathbf{q}_{\text{CDW}} \approx M$. The corresponding phonon linewidth, shown in Fig. 2(b), displays a strong enhancement near the M point, indicating substantial electron-phonon coupling for this specific phonon mode. The momentum dependence of the electronic susceptibility provides further insight into the origin of this instability. The imaginary part, $\text{Im}[\chi_0(\mathbf{q})]$, shown in Fig. 2(d), exhibits enhanced intensity over extended regions of the Brillouin zone, reflecting the overall geometry of the Fermi surface. However, its maxima are broadly distributed and do not uniquely coincide with the M point. In contrast, the real part, $\text{Re}[\chi_0(\mathbf{q})]$, presented in Fig. 2(c), shows pronounced peaks near the M point, consistent with the momentum location of the soft phonon mode.

The lack of a one-to-one correspondence between the peak positions of $\text{Re}[\chi_0(\mathbf{q})]$ and $\text{Im}[\chi_0(\mathbf{q})]$ indicates that simple Fermi-surface nesting is not the dominant driving mechanism for the CDW instability in Mo_2NF_2 . Instead, the coincidence of the phonon softening, the enhancement of $\text{Re}[\chi_0(\mathbf{q})]$, and the large phonon linewidth at the M point points to a CDW mechanism governed by strong momentum-dependent

electron–phonon coupling, rather than a purely electronic Peierls-type instability.

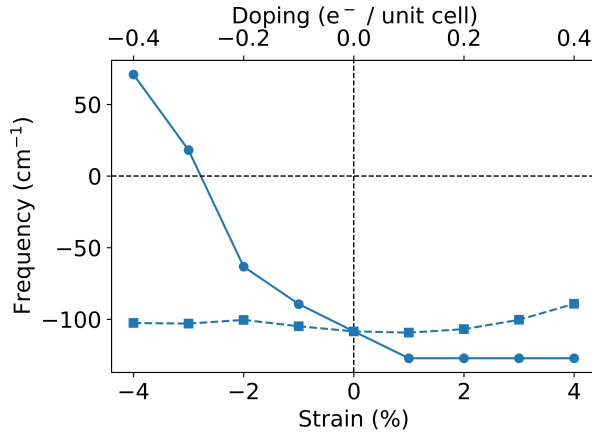


Figure 3: Evolution of the phonon frequency of the unstable mode at the M point as a function of biaxial strain and charge doping. The bottom horizontal axis shows the applied strain, while the top axis indicates the corresponding electron (positive) and hole (negative) doping per unit cell.

External perturbations provide an effective means to control lattice instabilities in low-dimensional materials. To assess possible routes for stabilizing the high-symmetry phase of Mo_2NF_2 , we examine the effects of biaxial strain and charge doping on the unstable soft phonon mode at the M point. In the unperturbed structure, the phonon spectrum exhibits an imaginary-frequency mode at the M point, indicating a dynamical lattice instability. Figure 3 summarizes the evolution of the phonon frequency of this mode under both biaxial strain and electron or hole doping. Negative phonon frequencies correspond to imaginary modes and reflect an unstable lattice configuration.

Charge doping, introduced by adding or removing electrons from the unit cell, has only a weak influence on the unstable phonon mode. As shown in Fig. 3, both electron and hole doping shift the phonon frequency marginally, but the mode remains imaginary over the entire doping range considered. This result indicates that modifying the electronic filling alone is insufficient to suppress the lattice instability. In contrast, biaxial strain has a pronounced effect on the soft phonon. Compressive strain progressively hardens the unstable mode, reducing the magnitude of the imaginary frequency. When the compressive strain exceeds approximately -3% , the phonon frequency at the M point becomes positive, signaling complete stabilization of the soft mode. Tensile strain, on the other hand, further destabilizes the lattice by enhancing the imaginary phonon frequency.

The markedly different responses to strain and doping highlight the dominant role of lattice degrees of freedom in governing the instability. The effectiveness of compressive strain in stabilizing the soft phonon suggests that the instability is primarily controlled by momentum-dependent lattice interactions rather than changes in electronic filling. These results demonstrate that external strain provides a viable and efficient route to suppress the unstable soft phonon and stabilize the high-symmetry phase in Mo_2NF_2 .

3.2 Charge-Density-Wave (CDW) Structural Distortion

The relaxed charge-density-wave (CDW) phase of Mo_2NF_2 exhibits pronounced atomic-scale lattice distortions involving all three atomic sublattices, as illustrated in Fig. 4. In contrast to the high-symmetry structure, the CDW phase is characterized by a periodic modulation of interatomic distances, reflecting the condensation of the unstable soft phonon mode at the M point. As shown in Fig. 4(a), the CDW distortion is not confined to a single atomic layer but instead involves correlated displacements of Mo, N, and F atoms along both in-plane and out-of-plane directions. This collective distortion underscores the

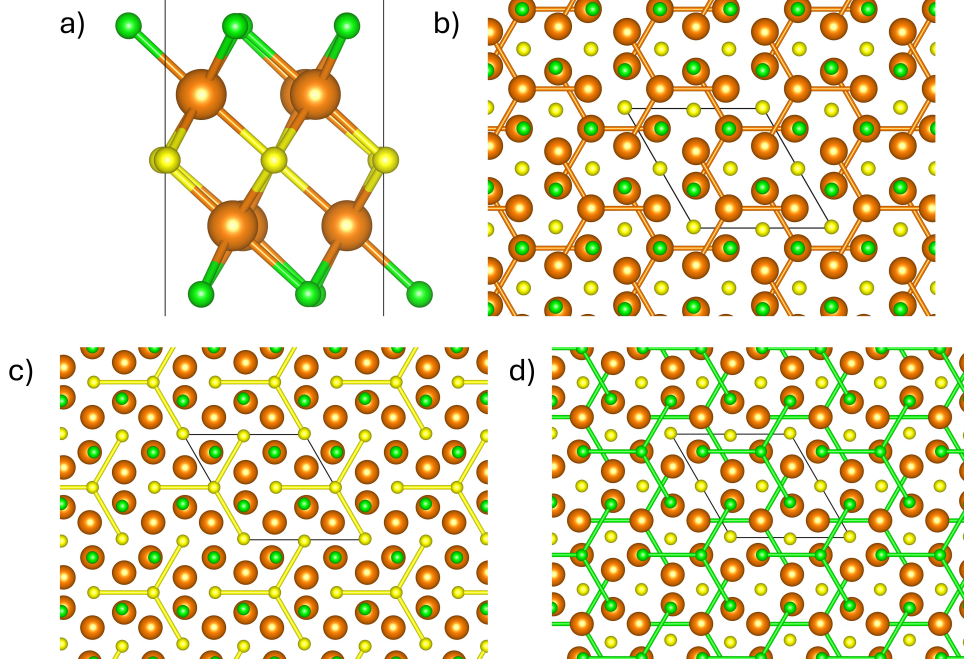


Figure 4: Atomic-scale structural characteristics of the charge-density-wave (CDW) phase in Mo_2NF_2 . (a) Side view of the CDW structure, showing lattice distortions involving the Mo, N, and F sublattices. (b) Top view highlighting the shortened Mo–Mo bonds in the CDW phase, with a representative bond length of 2.70 Å. (c) Top view illustrating the N–N bond modulation induced by the CDW, with a characteristic bond length of 2.72 Å. (d) Top view showing the corresponding F–F bond modulation in the CDW phase, also characterized by a bond length of 2.72 Å. Orange, yellow, and green spheres represent Mo, N, and F atoms, respectively.

strong coupling between the transition-metal framework and the surface terminations, highlighting the cooperative nature of the CDW instability in this Janus MXene. The CDW phase is energetically favored, exhibiting a total energy reduction of 25.78 meV/formula compared to the high-symmetry structure and 244.44 meV/formula compared to the -3% strain-stabilized high-symmetry phase.

The most prominent structural signature of the CDW appears in the Mo sublattice. Figure 4(b) reveals the formation of shortened Mo–Mo bonds with a representative bond length of 2.70 Å compared to HSS with bond length of 2.76 Å (Or 2.67 Å when applying -3% biaxial compressive strain), indicating a partial dimerization of Mo atoms driven by the CDW modulation. This Mo–Mo bond contraction is consistent with the dominant contribution of Mo d states near the Fermi level and reflects the central role of the Mo framework in stabilizing the CDW phase. In addition to the Mo sublattice, the CDW distortion induces measurable bond-length modulations in the anion sublattices. As shown in Fig. 4(c), the N atoms undergo a periodic rearrangement, leading to characteristic N–N bond lengths of approximately 2.72 Å. A similar modulation is observed for the F surface terminations, as illustrated in Fig. 4(d), where F–F bond lengths of about 2.72 Å are formed. These distortions indicate that the CDW involves a coherent reconstruction of the entire lattice rather than a purely metal-centered instability.

Overall, the emergence of bond-length alternation across the Mo, N, and F sublattices provides direct real-space evidence of the CDW state in Mo_2NF_2 . The multi-sublattice nature of the distortion, together with the associated phonon softening and enhanced electron–phonon coupling at the M point, confirms that the CDW phase is driven by a lattice instability with strong momentum-dependent coupling, rather than a simple electronic nesting mechanism.

The electronic structures of Mo_2NF_2 in the high-symmetry and charge-density-wave (CDW) phases are compared in Fig. 5. In the high-symmetry structure, the electronic band dispersion exhibits several

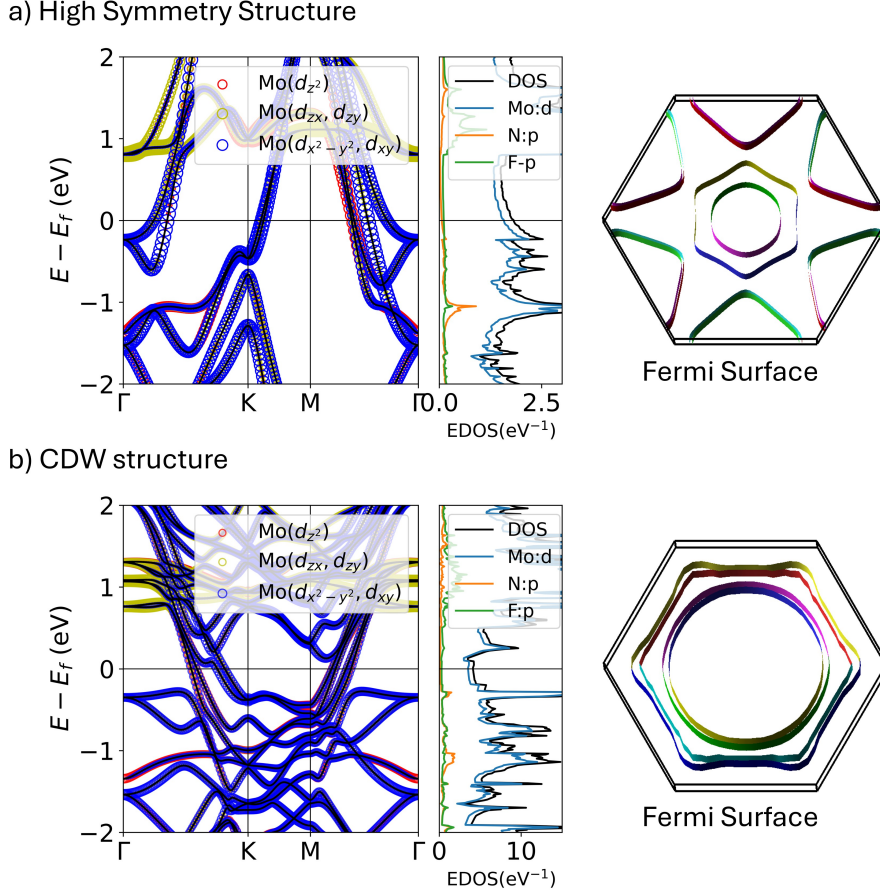


Figure 5: Electronic structure of Mo₂NF₂ in the high-symmetry and charge-density-wave (CDW) phases. (a) High-symmetry structure: orbital-projected electronic band structure along the high-symmetry path $\Gamma-K-M-\Gamma$, corresponding electronic density of states (EDOS), and Fermi surface. (b) CDW structure: orbital-projected band structure, EDOS, and Fermi surface of the relaxed CDW phase. The bands are colored according to the dominant Mo d -orbital contributions (d_{z^2} , d_{zx}/d_{zy} , and $d_{x^2-y^2}/d_{xy}$), while the EDOS is decomposed into Mo d , N p , and F p states. The transition from the high-symmetry phase to the CDW phase leads to pronounced band reconstruction and a substantial modification of the Fermi surface topology, reflecting the lattice distortion and Brillouin-zone folding associated with the CDW ordering.

bands crossing the Fermi level, resulting in a metallic character. Orbital-projected band analysis reveals that the states near the Fermi level are predominantly derived from Mo d orbitals, with the d_{z^2} and in-plane $d_{x^2-y^2}/d_{xy}$ components providing the largest contributions. The corresponding electronic density of states (EDOS) further confirms the dominance of Mo d states at low energies, while the N p and F p states contribute mainly at deeper binding energies. The Fermi surface of the high-symmetry phase displays hexagonally warped contours centered around the Brillouin-zone center, reflecting the underlying hexagonal lattice symmetry. These Fermi surface features give rise to extended regions with nearly parallel segments, suggesting the presence of partial nesting; however, the nesting is not associated with a single dominant wave vector. This observation is consistent with the absence of a purely electronic instability in the high-symmetry phase and supports the phonon-driven nature of the CDW instability discussed earlier.

Upon relaxation into the CDW phase, the electronic structure undergoes a substantial reconstruction, as shown in Fig. 5(b). The lattice distortion associated with the CDW leads to Brillouin-zone folding and the appearance of additional bands, resulting in a more complex band dispersion near the Fermi level.

Despite this reconstruction, the system remains metallic, with finite density of states at the Fermi energy. The redistribution of spectral weight among the Mo d orbitals indicates a strong coupling between the electronic states and the lattice distortion, particularly within the Mo sublattice. The CDW-induced structural modulation also produces a pronounced reshaping of the Fermi surface. Compared to the high-symmetry phase, the Fermi surface in the CDW phase becomes smoother and more circular, reflecting the reduced symmetry and band folding effects. The absence of a complete Fermi-surface gap further confirms that the CDW transition in Mo_2NF_2 does not originate from a simple Peierls-type instability. Instead, the observed electronic reconstruction is consistent with a lattice-driven CDW stabilized by strong momentum-dependent electron–phonon coupling, in agreement with the phonon softening and linewidth enhancement at the M point.

3.3 Competition between CDW and Superconductivity

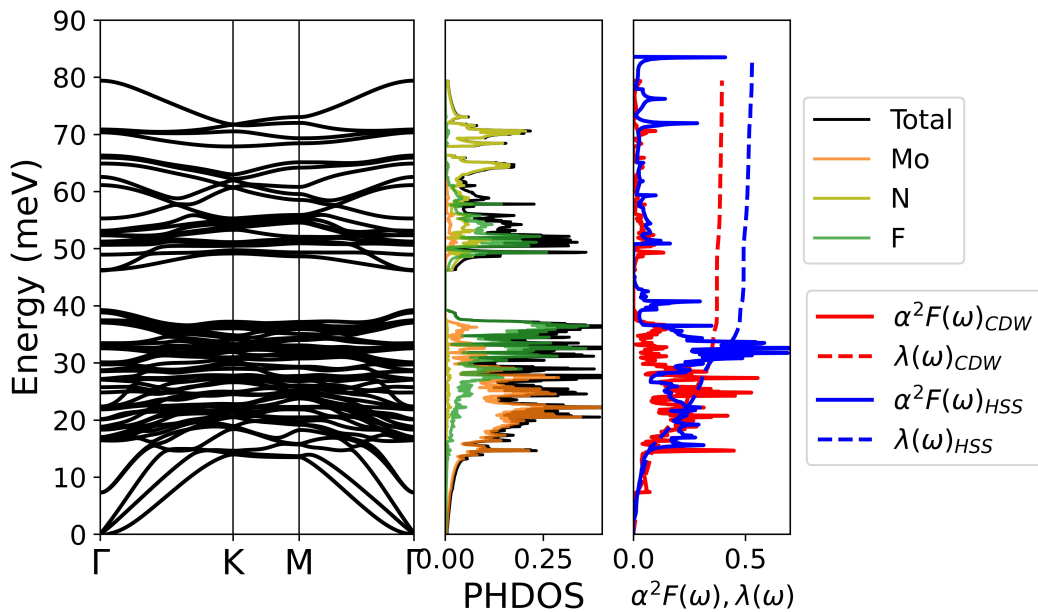


Figure 6: Phonon properties and electron–phonon coupling of Mo_2NF_2 in the charge-density-wave (CDW) phase and the strain-stabilized high-symmetry structure (HSS). Left panel: phonon dispersion of the relaxed CDW phase along the high-symmetry path Γ – K – M – Γ , showing the absence of imaginary phonon modes and confirming the dynamical stability of the CDW structure. Middle panel: projected phonon density of states (PHDOS), resolved into Mo (orange), N (yellow), and F (green) contributions. Right panel: Eliashberg spectral function $\alpha^2F(\omega)$ (solid lines) and the cumulative electron–phonon coupling constant $\lambda(\omega)$ (dashed lines). Red curves correspond to the CDW phase, yielding a total EPC constant $\lambda = 0.40$ and a logarithmic average phonon frequency $\omega_{\log} = 219$ K. Blue curves represent the high-symmetry structure stabilized under -3% compressive strain, with an enhanced EPC strength of $\lambda = 0.53$ and $\omega_{\log} = 272$ K.

The electron–phonon coupling (EPC) analysis reveals a clear competition between the charge-density-wave (CDW) phase and superconductivity in Mo_2NF_2 . As summarized in Fig. 6, the CDW phase is characterized by a moderate EPC constant of $\lambda = 0.40$ and a logarithmic average phonon frequency $\omega_{\log} = 219$ K, leading to an estimated superconducting transition temperature of $T_c \sim 1$ K. In contrast, the strain-stabilized high-symmetry structure (HSS) under -3% compressive strain exhibits a significantly enhanced EPC strength of $\lambda = 0.53$ and a higher $\omega_{\log} = 272$ K, resulting in an increased transition temperature of $T_c \sim 4$ K. The suppression of superconductivity in the CDW phase can be directly traced to the lattice reconstruction and phonon hardening associated with CDW formation. The condensation

of the soft phonon mode at the M point stabilizes the CDW structure but simultaneously removes low-energy phonon modes that would otherwise contribute strongly to the EPC. As a result, both the total EPC constant and the characteristic phonon frequency scale are reduced in the CDW phase, diminishing the pairing interaction required for superconductivity. Therefore, Kohn-like phonon softening driven by strong electron-phonon coupling can enhance phonon-mediated superconductivity when it occurs at an optimal level [34]. However, excessive softening that results in imaginary phonon modes signals the emergence of a charge-density-wave (CDW) instability, which in turn suppresses superconductivity.

Furthermore, the CDW-induced band folding and Fermi-surface reconstruction redistribute electronic spectral weight near the Fermi level, reducing the phase space available for Cooper pairing. Although the CDW phase remains metallic, the partial reconstruction of the electronic structure weakens the coupling between electrons and lattice vibrations, further suppressing superconductivity. This behavior highlights the antagonistic relationship between CDW order and superconductivity in Mo_2NF_2 .

In contrast, suppressing the CDW instability via compressive strain restores the high-symmetry lattice and stabilizes all phonon modes, thereby enhancing both λ and ω_{\log} . The resulting increase in T_c under strain demonstrates that superconductivity in Mo_2NF_2 is favored in the absence of CDW order and can be effectively tuned through external lattice control. These results establish Mo_2NF_2 as a representative example of a phonon-mediated superconductor in which superconductivity emerges upon suppression of a competing CDW phase, offering a promising platform for strain-engineered quantum phases in Janus MXenes.

4 Conclusions

In conclusion, we have demonstrated that Mo_2NF_2 hosts a pronounced charge-density-wave instability originating from a soft phonon mode at the M point. Through a combined analysis of phonon dispersions, phonon linewidths, electronic susceptibility, and real-space structural distortions, we establish that the CDW is driven by strong momentum-dependent electron-phonon coupling rather than a purely electronic nesting mechanism. The resulting CDW phase is characterized by cooperative lattice distortions involving the Mo framework as well as the N and F sublattices, confirming the collective nature of the instability in this Janus MXene.

Our results further reveal that external perturbations play markedly different roles in controlling the instability. While charge doping has only a marginal effect and fails to stabilize the soft phonon, moderate compressive biaxial strain efficiently suppresses the CDW by hardening the unstable mode. This strain-induced stabilization of the high-symmetry phase leads to a substantial enhancement of the electron-phonon coupling strength and the characteristic phonon energy scale. Importantly, the CDW phase is shown to suppress superconductivity by reducing both the electron-phonon coupling constant and the logarithmic average phonon frequency, resulting in a low superconducting transition temperature of approximately 1 K. Upon suppression of the CDW under compressive strain, superconductivity is significantly enhanced, with an estimated transition temperature of about 4 K. These findings highlight a clear competition between CDW order and superconductivity in Mo_2NF_2 and demonstrate that lattice control provides an effective pathway to tune emergent quantum phases.

Overall, this work establishes Janus MXenes as a versatile platform for exploring the interplay between lattice instabilities and superconductivity and suggests that strain engineering may offer a practical route to designing and optimizing superconducting states in two-dimensional materials.

Data Availability

The data that support the findings of this study are available from the corresponding authors upon reasonable request.

Code Availability

The first-principles DFT calculations were performed using the open-source Quantum ESPRESSO package, available at <https://www.quantum-espresso.org>, along with pseudopotentials from the Quantum ESPRESSO pseudopotential library at <https://pseudopotentials.quantum-espresso.org/>.

Acknowledgments

This research project is supported by the Second Century Fund (C2F), Chulalongkorn University. We acknowledge the supporting computing infrastructure provided by NSTDA, CU, CUAASC, NSRF via PMUB [B05F650021, B37G660013] (Thailand). (URL:www.e-science.in.th). This also work used the ARCHER2 UK National Supercomputing Service (<https://www.archer2.ac.uk>) as part of the UKCP collaboration.

Author Contributions

Jakkapat Seeyangnok performed all calculations, analyzed the results, wrote the initial draft of the manuscript, and coordinated the project. Graeme J. Ackland and Udomsilp Pinsook contributed to the analysis of the results and to the writing the manuscript.

References

- [1] George Gruner. *Density waves in solids*. CRC press, 2018.
- [2] Rudolf Ernst Peierls. *Quantum theory of solids*. Oxford University Press, 1955.
- [3] W Kohn. Image of the fermi surface in the vibration spectrum of a metal. *Physical Review Letters*, 2(9):393, 1959.
- [4] MD Johannes and II Mazin. Fermi surface nesting and the origin of charge density waves in metals. *Physical Review B—Condensed Matter and Materials Physics*, 77(16):165135, 2008.
- [5] Xuetao Zhu, Jiandong Guo, Jiandi Zhang, and EW Plummer. Misconceptions associated with the origin of charge density waves. *Advances in Physics: X*, 2(3):622–640, 2017.
- [6] José Ángel Silva-Guillén, Pablo Ordejón, Francisco Guinea, and Enric Canadell. Electronic structure of 2h-nbse2 single-layers in the cdw state. *2D Materials*, 3(3):035028, 2016.
- [7] F Weber, S Rosenkranz, J-P Castellan, R Osborn, R Hott, R Heid, K-P Bohnen, T Egami, AH Said, and D Reznik. Extended phonon collapse and the origin of the charge-density wave in 2 h-nbse 2. *Physical review letters*, 107(10):107403, 2011.
- [8] Miguel M Ugeda, Aaron J Bradley, Yi Zhang, Seita Onishi, Yi Chen, Wei Ruan, Claudia Ojeda-Aristizabal, Hyejin Ryu, Mark T Edmonds, Hsin-Zon Tsai, et al. Characterization of collective ground states in single-layer nbse 2. *Nature Physics*, 12(1):92–97, 2016.

- [9] Yuki Nakata, Katsuaki Sugawara, Ashish Chainani, Hirofumi Oka, Changhua Bao, Shaohua Zhou, Pei-Yu Chuang, Cheng-Maw Cheng, Tappei Kawakami, Yasuaki Saruta, et al. Robust charge-density wave strengthened by electron correlations in monolayer 1t-tase2 and 1t-nbse2. *Nature communications*, 12(1):5873, 2021.
- [10] Xiaoxiang Xi, Liang Zhao, Zefang Wang, Helmuth Berger, László Forró, Jie Shan, and Kin Fai Mak. Strongly enhanced charge-density-wave order in monolayer nbse2. *Nature nanotechnology*, 10(9):765–769, 2015.
- [11] Amir Dalal, Jonathan Ruhman, and Jörn WF Venderbos. Flat band physics in the charge-density wave state of 1 t-tas2 and 1 t-tase2. *npj Quantum Materials*, 10(1):31, 2025.
- [12] Adam W Tsen, Robert Hovden, Dennis Wang, Young Duck Kim, Junichi Okamoto, Katherine A Spoth, Yu Liu, Wenjian Lu, Yuping Sun, James C Hone, et al. Structure and control of charge density waves in two-dimensional 1t-tas2. *Proceedings of the National Academy of Sciences*, 112(49):15054–15059, 2015.
- [13] Sharon S Philip, Joerg C Neufeind, Matthew B Stone, and Despina Louca. Local structure anomaly with the charge ordering transition of 1 t-tas 2. *Physical Review B*, 107(18):184109, 2023.
- [14] Matteo Calandra and Francesco Mauri. Charge-density wave and superconducting dome in tise 2 from electron-phonon interaction. *Physical review letters*, 106(19):196406, 2011.
- [15] Ruiqi Ku, Luo Yan, Jian-Guo Si, Songyuan Zhu, Bao-Tian Wang, Yadong Wei, Kaijuan Pang, Weiqi Li, and Liujiang Zhou. Ab initio investigation of charge density wave and superconductivity in two-dimensional janus 2 h/1 t-mosh monolayers. *Physical Review B*, 107(6):064508, 2023.
- [16] M Munib ul Hassan Noor ul Taqi, Udomsilp Pinsook, and Jakkapat Seeyangnok. Superconductivity and phase stability in various combinations of janus mosh bilayers. *Physica Scripta*, 100(5):055939, 2025.
- [17] Chang-Hao Sui, Shu-Xiang Qiao, Hao Ding, Kai-Yue Jiang, Shu-Ying Shang, and Hong-Yan Lu. Two-dimensional janus moseh with tunable charge density wave, superconductivity and topological properties. *Materials Today Physics*, 53:101698, 2025.
- [18] Jakkapat Seeyangnok, Udomsilp Pinsook, and Graeme J Ackland. Charge density wave order and superconductivity in janus moxh monolayers. *arXiv preprint arXiv:2601.02959*, 2026.
- [19] Jakkapat Seeyangnok, M Munib Ul Hassan, Udomsilp Pinsook, and Graeme Ackland. Superconductivity and electron self-energy in tungsten-sulfur-hydride monolayer. *2D Materials*, 11(2):025020, 2024.
- [20] Jakkapat Seeyangnok, Udomsilp Pinsook, and Graeme J Ackland. Superconductivity and strain-enhanced phase stability of janus tungsten chalcogenide hydride monolayers. *Physical Review B*, 110(19):195408, 2024.
- [21] Shu-Xiang Qiao, Kai-Yue Jiang, Chang-Hao Sui, Peng-Cheng Xiao, Na Jiao, Hong-Yan Lu, and Ping Zhang. Prediction of charge density wave, superconductivity and topology properties in two-dimensional janus 2h/1t-wxh (x= s, se). *Materials Today Physics*, 46:101485, 2024.
- [22] Jingyu Li, Liuming Wei, Xianbiao Shi, Lanting Shi, Jianguo Si, Peng-Fei Liu, and Bao-Tian Wang. Machine learning accelerated discovery of superconducting two-dimensional janus transition metal sulfhydrates. *Physical Review B*, 109(17):174516, 2024.

- [23] M Munib ul Hassan Noor ul Taqi and Udomsilp Pinsook. Superconductivity in monolayer janus titanium-sulfurhydride (tish) at ambient pressure. *Journal of Physics: Condensed Matter*, 36(32):325702, 2024.
- [24] Jakkapat Seeyangnok, Udomsilp Pinsook, and Graeme J Ackland. Competition between superconductivity and ferromagnetism in 2d janus mxh (m= ti, zr, hf, x= s, se, te) monolayer. *Journal of Alloys and Compounds*, 1033:180900, 2025.
- [25] Jakkapat Seeyangnok and Udomsilp Pinsook. Enhanced and tunable superconductivity enabled by mechanically stable halogen-functionalized mo2c mxenes, 2026.
- [26] Paolo Giannozzi, Stefano Baroni, Nicola Bonini, Matteo Calandra, Roberto Car, Carlo Cavazzoni, Davide Ceresoli, Guido L Chiarotti, Matteo Cococcioni, Ismaila Dabo, et al. Quantum espresso: a modular and open-source software project for quantum simulations of materials. *Journal of physics: Condensed matter*, 21(39):395502, 2009.
- [27] John P Perdew, Kieron Burke, and Matthias Ernzerhof. Generalized gradient approximation made simple. *Physical review letters*, 77(18):3865, 1996.
- [28] Martin Schlipf and François Gygi. Optimization algorithm for the generation of oncv pseudopotentials. *Computer Physics Communications*, 196:36–44, 2015.
- [29] Hendrik J Monkhorst and James D Pack. Special points for brillouin-zone integrations. *Physical review B*, 13(12):5188, 1976.
- [30] MPAT Methfessel and AT Paxton. High-precision sampling for brillouin-zone integration in metals. *physical review B*, 40(6):3616, 1989.
- [31] Stefano Baroni, Stefano De Gironcoli, Andrea Dal Corso, and Paolo Giannozzi. Phonons and related crystal properties from density-functional perturbation theory. *Reviews of modern Physics*, 73(2):515, 2001.
- [32] Ph B Allen and RC Dynes. Transition temperature of strong-coupled superconductors reanalyzed. *Physical Review B*, 12(3):905, 1975.
- [33] Udomsilp Pinsook, Nattawut Natkunlaphat, Komkrit Rientong, Pakin Tasee, and Jakkapat Seeyangnok. Analytic solutions of eliashberg gap equations at superconducting critical temperature. *Physica Scripta*, 99(6):065211, 2024.
- [34] Cunyuan Jiang, Enrico Beneduce, Matteo Baggioli, Chandan Setty, and Alessio Zaccone. Possible enhancement of the superconducting t_c due to sharp kohn-like soft phonon anomalies. *Journal of Physics: Condensed Matter*, 35(16):164003, 2023.